



Oscillation Analysis for Longitudinal Dynamics of a Fixed-Wing UAV Using PID Control Design

B. K. Aliyu^{1*}, C. A. Osheku¹, P. N. Okeke², F. E. Opara² and B. I. Okere²

¹Centre for Space Transport and Propulsion (CSTP), Epe Lagos-State, Nigeria.

²Centre for Basic Space Science (CBSS), Nsukka Enugu-State, Nigeria.

Authors' contributions

This work was carried out in collaboration between all authors. Author BKA designed the study, did the first Simulations in MATLAB/Simulink and wrote the first draft of the manuscript. Author BIO verified all DATCOM and MATLAB result. Authors CAO, PNO and FEO edited the first draft of the manuscript, verified all results, and managed information release and literature searches. All authors read and approved the final manuscript.

Article Information

DOI: 10.9734/AIR/2015/18334

Editor(s):

(1) Akash Dixit, Department of Mechanical Engineering, Oakland University, USA.

Reviewers:

(1) Anonymous, Kielce University of Technology, Poland.

(2) Khairul Nizam Tahar, Universiti Teknologi Mara, Shah Alam, Malaysia.

(3) Anonymous, Inha University, Korea.

(4) Anonymous, Tongji University, China.

(5) Anonymous, Dalian University of Technology, China.

Complete Peer review History: <http://sciencedomain.org/review-history/9899>

Original Research Article

Received 15th April 2015

Accepted 5th June 2015

Published 20th June 2015

ABSTRACT

A longitudinally disturbed motion of a UAV after an arbitrary initial disturbance consists normally of two oscillatory modes: the *short-period* oscillation and the *phugoid oscillation*. The typical longitudinal model of a UAV in state-space can be separated into *short-period* mode and *phugoid period* mode equations of motion. In this study, we choose to investigate the dynamic characteristics of the longitudinal dynamic equation of a mini-UAV and its reduced forms popularly known as *short-period* and *phugoid period* modes. This is necessary to establish a basis for plant selection during PID autopilot design. The *short* and *phugoid* period oscillations modes are sieved from the longitudinal dynamic equation and carry the same eigenvalues of the longitudinal model, but they still differ. Firstly, the three systems have different *step* response trajectories due to their different *DC* gain values. Secondly, the variables that constitute the *short-period* and *phugoid mode* dynamic equations can be identified by their *settling time* after designing PID controllers. State-space model of the longitudinal dynamics, phugoid mode and short period dynamics of a UAV can

*Corresponding author: E-mail: aliyu_bhar@yahoo.com;

be transformed into equivalent transfer functions. These transfer functions are then used in the design of Proportional, Integral and Derivative (PID) controllers. Hence, the *phugoid* mode variables are the system variables in the longitudinal dynamic model with the longest *settling time*. The *short period* mode variables are the longitudinal system variables with the shortest *settling time*. Synthesis and simulation were done in MATLAB/Simulink. Also, from simulation results, plant for autopilot design could be selected based on the system with smallest *rise time*.

Keywords: UAV; PID control; MATLAB/Simulink; time response characteristics; short period mode; phugoid mode.

1. INTRODUCTION

High cost and operational limitation of manned aircraft prohibits their use by a lot of scientific institutions as platforms for research. The use of Unmanned Aerial Vehicles (UAV) offers a viable alternative. The lack of neither human pilot on board nor a pilot on the ground in a control centre (Ground Control Station) allows a significantly smaller, lighter and less expensive aircraft to be developed. Most importantly, the unmanned nature relaxes the aircraft's flight safety margin. While many operational UAV's exist, a good number of them are limited to military applications and are largely unavailable to civilian research institutions. A lot of papers have been published by the academic community documenting their own research into the design and flight testing of inexpensive UAVs. Few of these projects are intended for use outside their own research departments. However the growing knowledge base and success of many of these projects, points to the fact that a uniquely built UAV may be realistically developed by the National Space Research and Development Agency (NASRDA) of Nigeria, tailored to their specific mission profile and environment [1]. An important task for the development of UAV flight test platforms is modelling and identifying the aircraft dynamics. Accurate models of UAV flight dynamics are generally unavailable due to the custom design of the airframes. However, such models are required to characterize aircraft behaviour and determine stability and performance properties before designing a controller. Two of the most important calculations needed for an airplane are the coefficient of lift and drag, which put limitations on the airplane's aerodynamic performance, thereby also affecting the power and thrust requirement [2].

One of the primary functions of an autopilot is the ability to control the UAV response to match command parameters. This ability is largely

determined by the performance of the control algorithm implemented by the autopilot software. All autopilots reviewed for UAVs state that their control algorithm uses the well-established proportional, integral, derivative (PID) controller [3,4,5,6]. The Proportional-Integral-Derivative (PID), controller dates back to 1890s, with the first practical example from 1911 (largely owing to Elmer Sperry's ship autopilot) [7].

The development of an autopilot system is an area undergoing intense research. The ability to test autopilots in a virtual (software) environment using a software flight dynamics model for UAV's is significant for this study. In many cases, testing newly developed autopilot systems in a virtual environment is the only way to guarantee absolute safety. Additionally the model will allow better repeatability in testing with controlled environment.

In this study, we are careful enough to show that the plant used in the design of PID autopilots system for a mini-UAV will have different time response characteristic(s) depending on how the variable is defined in transfer function. This could be from a longitudinal dynamics model or from a reduced model (short period dynamics, or phugoid mode). In most literatures, no scientific reason is given for such plant selection [8].

The mini-UAV, Ultra Stick 25e chosen for this research is commercially available and serves as the primary flight test vehicle for the University of Minnesota UAV flight control research group. The UltraStick 25e is a small, low-cost, fixed-wing, radio controlled aircraft. It is equipped with conventional elevator, aileron, and rudder control surfaces. The aircraft is powered by an electric motor that drives a propeller.

The basic physical characteristics of the UAV are as outlined in Table 1. A UAV falls into the category of the mini type if it has a wingspan of less than 2 m.

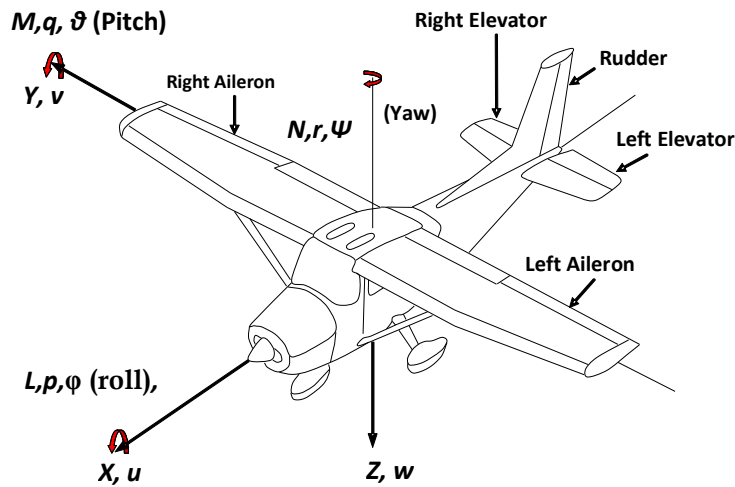


Fig. 1. 6 DoF variables of the Ultrastick 25e mini-UAV

Table 1. UAV parameters

Parameter	Description	Value and units
A	Wing reference Area	0.31 m^2
b	Wing span	1.27 m
\bar{c}	Wing chord	0.25 m
m	Gross weight	1.9 kg
m_c	Mass of payload	0.25 kg
m_T	Take off mass	2.15 kg

This paper is organized as follows: a Longitudinal fixed-wing aircraft flight dynamics model structure is presented in 2.0, hence, *phugoid* mode dynamics model and *short period* dynamics model are extracted from the Longitudinal model. Section 3.0 introduces the PID controller. Design and simulation to define *short period* and *phugoid* dynamics where outlined in section 4.0.

2. LONGITUDINAL FIXED-WING AIRCRAFT FLIGHT DYNAMICS

Numerical modelling of flight dynamics has a long history in aerospace industry, and is used in the development of all modern aircrafts. A flight dynamics model is a mathematical representation of the steady state performance and dynamic response that is expected of the proposed vehicle.

The fundamental goal of flight dynamics modelling is to represent the flight motion numerically for a given input. This is expected to be close to the flight motion in the real world as the application requires. All flight dynamics models are based on the mathematical model derived from Newtonian Physics. From Newton's second law, an aircraft's motion in its six-degrees-of-freedom (6DOF) can be described by a system of non-linear first order differential equations. These equations of motion served as the fundamental for almost all flight dynamics model. With today's computing power, the processing time of solving these equations is trivial comparing to other signal processing algorithms (e.g. Kalman filter) that might be implemented as part of the flight model.

A nonlinear aircraft model built in Simulink was linearized at forward velocity, $u=17 \text{ m/s}$, pitch angle, $\theta=0.0217 \text{ rad}$, elevator deflection angle, $\eta = 0.091 \text{ rad}$, throttle angle, $\tau = 0.559 \text{ rad}$, and altitude $h = 120 \text{ m}$. The simplest form of the equations of motion is taken in the body axis reference frame of the aircraft and assumes an Earth coordinate system. Twelve states are required to describe the aircraft rigid-body longitudinal dynamics, these are: three inertial positions (X, Y, Z), three body-axis velocities (u, v, w), three attitude angles (ϕ, θ, φ), and three body-axis angular rates (p, q, r). The coupled (longitudinal and lateral) 6DoF equation of motion for a rigid aircraft is given as [9];

$$m\dot{u} - \dot{X}_u u - \dot{X}_v v - \dot{X}_w w - \dot{X}_p p - \left(\dot{X}_q - mW_e \right) q - \dot{X}_r r + \quad (1)$$

$$mg\theta \cos \theta_e = \dot{X}_\xi \xi + \dot{X}_\eta \eta + \dot{X}_\zeta \zeta + \dot{X}_\tau \tau,$$

$$-\dot{Y}_u u + m\dot{v} - \dot{Y}_v v - \dot{Y}_w w - \dot{Y}_p p - \left(\dot{Y}_q + mW_e \right) q - \left(\dot{Y}_r - mU_e \right) r - mg\phi \cos \theta_e - \quad (2)$$

$$mg\psi \sin \theta_e = \dot{Y}_\xi \xi + \dot{Y}_\eta \eta + \dot{Y}_\zeta \zeta + \dot{Y}_\tau \tau,$$

$$-\dot{Z}_u u + \dot{Z}_v v + \left(m - \dot{Z}_w \right) \dot{w} - \dot{Z}_p p - \left(\dot{Z}_q + mU_e \right) q - \dot{Z}_r r - \quad (3)$$

$$mg\theta \sin \theta_e = \dot{Z}_\xi \xi + \dot{Z}_\eta \eta + \dot{Z}_\zeta \zeta + \dot{Z}_\tau \tau,$$

$$-\dot{L}_u u - \dot{L}_v v - \dot{L}_w w - L_p p - L_q q - \dot{L}_r r + I_x \dot{p} - I_{xz} \dot{r} = \dot{L}_\xi \xi + \dot{L}_\eta \eta + \dot{L}_\zeta \zeta + \dot{L}_\tau \tau, \quad (4)$$

$$-\dot{M}_u u - \dot{M}_v v - \dot{M}_w w - \dot{M}_p p - \dot{M}_q q - \dot{M}_r r + I_y \dot{q} = \dot{M}_\xi \xi + \dot{M}_\eta \eta + \dot{M}_\zeta \zeta + \dot{M}_\tau \tau, \quad (5)$$

$$-\dot{N}_u u - \dot{N}_v v - \dot{N}_w w - \dot{N}_p p - \dot{N}_q q - \dot{N}_r r - I_{xz} \dot{p} + I_z \dot{r} = \dot{N}_\xi \xi + \dot{N}_\eta \eta + \dot{N}_\zeta \zeta + \dot{N}_\tau \tau, \quad (6)$$

$$\dot{\phi} = p + (q \sin \phi + r \cos \phi) \tan \theta, \quad (7)$$

$$\dot{\theta} = q \cos \phi - r \sin \phi, \quad (8)$$

$$\dot{\psi} = \frac{q \sin \phi + r \cos \phi}{\cos \theta}, \quad (9)$$

where, m is the mass of the UAV, u, v, w are the velocity components in x, y, z axis respectively. η, ξ, ζ are notations for the control surfaces elevator, aileron and rudder respectively. X, Y, Z are forces in x, y, z direction and L, M, N are moments in the same axis coordinated. θ, ϕ, ψ are the three Euler angles of pitch, roll and yaw respectively. While I_x, I_y and I_z are moment of inertia in roll, pitch and yaw respectively, while I_{xy}, I_{xz} and I_{yz} are the products of inertia in the appropriate axis. For pitch control, we need a longitudinal dynamics equations, thus (1)-(9) needs to be decoupled to isolate the longitudinal dynamic equation of motion, these are (1), (3), (5) and (8). Decoupled longitudinal motion means that the aerodynamic coupling derivatives (dimensional) are negligibly small and may be taken as zero whence

$$\dot{X}_v = \dot{X}_p = \dot{X}_r = \dot{Z}_v = \dot{Z}_p = \dot{Z}_r = \dot{M}_v = \dot{M}_p = \dot{M}_r = 0. \quad (10)$$

Similarly, since aileron and rudder deflections do not usually cause motion in the longitudinal plane of symmetry the coupling aerodynamic control derivatives (dimensional) may also be taken as zero, thus

$$\dot{X}_\xi = \dot{X}_\zeta = \dot{Z}_\xi = \dot{Z}_\zeta = \dot{M}_\xi = \dot{M}_\zeta = 0. \quad (11)$$

Hence, the longitudinal dynamics (1), (3),(5) and (8) could be written as,

$$m\dot{u} - \dot{X}_u u - \dot{X}_w w - \dot{X}_q q + mg\theta \cos \theta_e = \dot{X}_\eta \eta + \dot{X}_\tau \tau, \quad (12)$$

$$-\dot{Z}_u u + \left(m - \dot{Z}_w\right) \dot{w} - \dot{Z}_w w - \left(\dot{Z}_p + mU_e\right) q + mg\theta \sin \theta_e = \dot{Z}_\eta \eta + \dot{Z}_\tau \tau, \quad (13)$$

$$-\dot{M}_u u - \dot{M}_w w - \dot{M}_q q + I_y \dot{q} = \dot{M}_\eta \eta + \dot{M}_\tau \tau, \quad (14)$$

$$\dot{\theta} = q \cos \varphi - r \sin \varphi, \quad (15) \quad \text{The characteristic equation for (17) is given in (18) and the roots are given in (19)}$$

The primary control surface in the longitudinal dynamics model is the elevator deflection η (rad), in state-space (12)-(15) can be represented as

$$\begin{bmatrix} \dot{u} \\ \dot{w} \\ \dot{q} \\ \dot{\theta} \end{bmatrix} = \begin{bmatrix} x_u & x_w & x_q & x_\theta \\ z_u & z_w & z_q & z_\theta \\ m_u & m_w & m_q & m_\theta \\ 0 & 0 & 1 & 0 \end{bmatrix} \begin{bmatrix} u \\ w \\ q \\ \theta \end{bmatrix} + \begin{bmatrix} x_\eta & x_\tau \\ z_\eta & z_\tau \\ m_\eta & m_\tau \\ 0 & 0 \end{bmatrix} \begin{bmatrix} \eta \\ \tau \end{bmatrix}, \quad (16)$$

where x_u , z_u and m_u are the dimensionless stability aerodynamic derivatives with respect to the state variable u , and x_η , z_η , and m_η are the dimensionless control aerodynamic derivatives. $\tau(t)$ is the throttle lever angle, if the UAV's cruise speed is constant, then $\dot{\tau} = 0$. Thus attitude can be controlled using the elevator η . For this study, the mini UAV pitch model was obtained after running the MATLAB script from [10], with our working conditions for linearization, this gave

$$\dot{x} = \begin{bmatrix} -0.7401 & 0.646 & -0.4834 & -9.778 \\ -0.6393 & -9.281 & 21.45 & -0.2225 \\ 1.081 & -10.04 & -21.35 & 0 \\ 0 & 0 & 1 & 0 \end{bmatrix} x + \begin{bmatrix} 0.74 \\ -4.52 \\ -244.2 \\ 0 \end{bmatrix} \eta \quad (17)$$

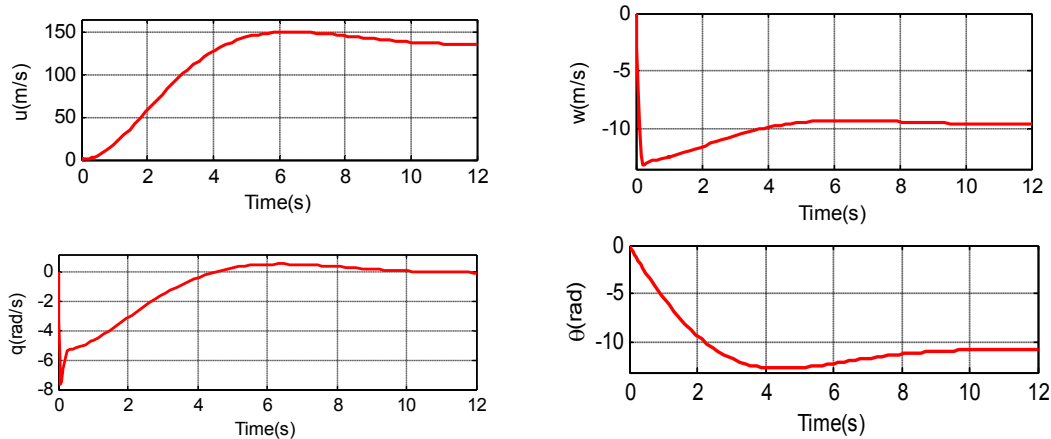


Fig. 2. Open-loop response of the longitudinal dynamics model

$$|A - \lambda I| = \lambda^4 + 31.37\lambda^3 + 437.11\lambda^2 + 316.16\lambda \quad (18)$$

$$\lambda = \begin{bmatrix} -15.32 \pm 13.4i \\ -0.37 \pm 0.499i \end{bmatrix}. \quad (19)$$

The DC gain for the four-state longitudinal model given in (17) was computed using MATLAB and has its values given in (20). This is necessary for accurate determination of the open-loop response of the system.

$$k = -CA^{-1}B = [136.5 \quad -9.6 \quad 0 \quad -10.9]^T. \quad (20)$$

A longitudinally disturbed motion of an UAV, following an arbitrary initial disturbance, consists normally of two oscillatory modes: the *short-period* oscillation and the *phugoid* oscillation. The disturbed flight consists initially of both *short-period* and *phugoid* modes but, after a comparatively short time, the former is normally damped out and the latter only persists for quite a long time. The *short-period* oscillation can, therefore, be only studied during the early stage of the disturbed flight [11].

2.1 Phugoid Mode

The phugoid mode is slow, well damped, and dominates the response in states u and θ . This mode can be represented as;

$$\begin{bmatrix} \dot{u} \\ \dot{\theta} \end{bmatrix} = \begin{bmatrix} x_u & x_\theta \\ -z_u/u_0 & 0 \end{bmatrix} \begin{bmatrix} u \\ \theta \end{bmatrix} + \begin{bmatrix} x_\eta \\ 0 \end{bmatrix} \eta, \equiv \dot{x} = \begin{bmatrix} -0.7401 & -9.778 \\ 0.0376 & 0 \end{bmatrix} x + \begin{bmatrix} 0.74 \\ 0 \end{bmatrix} \eta \quad (21)$$

The characteristic equation for the *phugoid* mode in (21) is given in (22) and roots in (23).

$$\lambda_{ph}^2 - x_u \lambda_{ph} - \frac{x_\theta}{u_0} z_u = 0, \equiv \lambda_{ph}^2 + 0.7401 \lambda_{ph} + 0.368 = 0. \quad (22)$$

$$\lambda_{ph} = \lambda_R \pm \lambda_I = -0.37 \pm 0.48i. \quad (23)$$

The natural frequency ω_n , for the phugoid mode is directly obtainable from the third term of (22) or from (23), in general form it is represented as,

$$\omega_{n_{ph}} = \sqrt{-\frac{x_\theta}{u_0} z_u} = \sqrt{\lambda_R^2 + \lambda_I^2} = 0.61 \text{sec}^{-1}. \quad (24)$$

The *phugoid oscillation* has a period of the order of one minute (up to 2 minutes or more at very high speeds). Hence, for this study, the phugoid period τ_{ph} was computed as,

$$\tau_{ph} = \frac{2\pi}{\omega_{n_{ph}}} = 10.3s. \quad (25)$$

Its damping factor ζ_{ph} , depend on a great number of derivatives, and there are considerable difficulties in correlating calculated and measured characteristics. Here, it was computed as,

$$\zeta_{ph} = \frac{-x_u}{2\omega_{n_{ph}}} = \frac{-\lambda_R}{\omega_n} = 0.61. \quad (26)$$

The *DC* gain for the phugoid mode dynamics is computed in (27) and its open-loop response is depicted in Fig. 3.

$$k_{ph} = -CA^{-1}B = [0.0 \quad 0.0757]^T \quad (27)$$

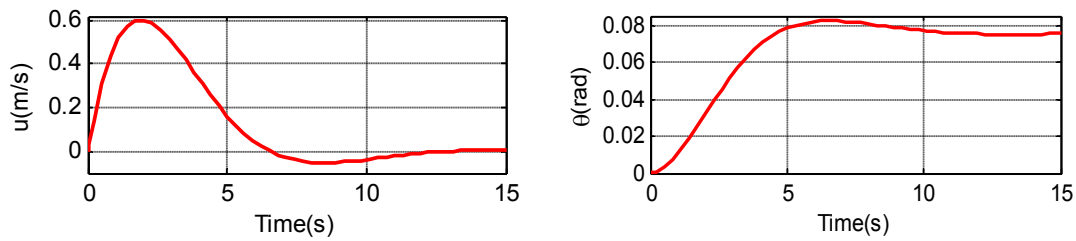


Fig. 3. Open loop response for the *phugoid* mode dynamics

2.2 Short Period Mode

The *short-period* mode is typically fast, moderately damped, and dominates the response in states w and q . Stability properties and pilot handling qualities of the aircraft depend primarily on the dynamics of the *short-period* mode. The *short-period* model takes the form,

$$\begin{bmatrix} \dot{w} \\ \dot{q} \end{bmatrix} = \begin{bmatrix} z_w & z_q \\ m_w & m_q \end{bmatrix} \begin{bmatrix} w \\ q \end{bmatrix} + \begin{bmatrix} z_\eta \\ m_\eta \end{bmatrix} \eta, \equiv \dot{x} = \begin{bmatrix} -9.28 & 21.45 \\ -10.04 & -21.35 \end{bmatrix} x + \begin{bmatrix} -4.52 \\ -244.2 \end{bmatrix} \eta. \quad (28)$$

The characteristic equation for the short period mode is given in (29) and the roots in (30).

$$\lambda_{sh}^2 + m_q \lambda_{sh} + z_w \lambda_{sh} + z_w m_q + m_w z_q = 0, \equiv \lambda_{sh}^2 + 30.63\lambda + 413.4860 = 0. \quad (29)$$

$$\lambda_{sh} = -15.31 \pm 13.4i \quad (30)$$

The natural frequency for the *short period* mode is represented and computed as follows;

$$\omega_{n_{sh}} = \sqrt{z_w m_q + m_w z_q} = 20.33 \text{sec}^{-1}, \quad (31)$$

The *short-period* oscillation has a period no more than a few seconds (sometimes below 1 second), and for this study it was computed as,

$$\tau_{sh} = \frac{2\pi}{\omega_{n_{sh}}} = 0.31s. \quad (32)$$

The short period oscillation is usually strongly damped to the extent that it may become not recordable after two or three periods, except for the dangerous cases of inadequate damping. The properties of this oscillation depend practically on only a few very important dimensionless aerodynamic derivatives, these are, z_w , m_w , m_q and $m_{\dot{w}}$. The damping factor is computed as,

$$\zeta_{sh} = \frac{m_q + z_w}{2\omega_{n_{sh}}} = 0.75. \quad (33)$$

Hence, *DC* gain for the *short period* dynamics is computed as,

$$k_{sh} = -CA^{-1}B = [-12.9015 \quad -5.3709]^T \quad (34)$$

The natures of the fast and slow modes are obvious if we view their dynamics separately as done here. It is interesting that this phenomenon could be illusive if one has only the longitudinal model to play with. *Step* response of the longitudinal dynamics does not reveal these

modes as seen in above Fig. 2 (all variables *settle* at about the same time).

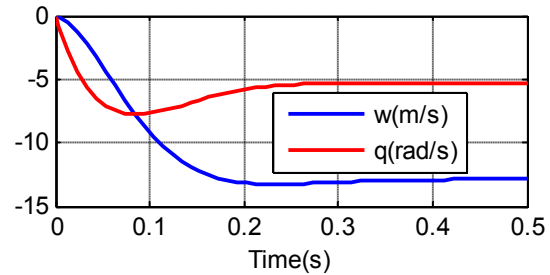


Fig. 4. Open-loop step response for the short period dynamics

3. PROPORTIONAL- INTEGRAL-DERIVATIVE (PID) CONTROL

PID controller is a linear controller, but has been used on nonlinear systems such as for an UAV fixed-wing [12]. The aim of a PID controller is to make the error signal, i. e., the difference between the reference signal and the measured signal, as small as possible, i.e. go to zero with time [13]. This is expressed mathematically as

$$\lim_{t \rightarrow \infty} e = \lim_{t \rightarrow \infty} r - y \rightarrow 0, \quad (35)$$

where, r is the reference signal and y is the measured signal from the sensor and for this study, sensor gain is taken as unity.

Mathematically, the PID controller designed in this study is described as:

$$\eta = K_p e(t) + K_i \int_0^t e(\tau) d\tau + K_d \frac{d}{dt} e(t), \quad (36)$$

where K_p , K_i and K_d represents the proportional, integral and derivative gains respectively, and η is the control signal. In other to design a PID controller, the mathematical model of the system to be controlled must be in transfer function.

Hence the MATLAB function `ss2tf` [14] was employed in this study to get state transfer functions from the longitudinal dynamics model described in (17), these are;

$$G_{u_L}(s) = \frac{u(s)}{\eta(s)} = \frac{s^3 + 138s^2 + 321s + 21751}{s^4 + 31.3711s^3 + 437.1129s^2 + 316.1637s + 159.3632}, \quad (37)$$

$$G_{w_L}(s) = \frac{w(s)}{\eta(s)} = \frac{-5s^3 - 5338s^2 - 3965s - 1534}{s^4 + 31.3711s^3 + 437.1129s^2 + 316.1637s + 159.3632}, \quad (38)$$

$$G_{q_L}(s) = \frac{q(s)}{\eta(s)} = \frac{-244s^3 - 2401s^2 - 1736s}{s^4 + 31.3711s^3 + 437.1129s^2 + 316.1637s + 159.3632}, \quad (39)$$

$$G_{\theta_L}(s) = \frac{\theta(s)}{\eta(s)} = \frac{-244s^2 - 2401s - 1736}{s^4 + 31.3711s^3 + 437.1129s^2 + 316.1637s + 159.3632}. \quad (40)$$

For the four transfer functions (37)-(40), we will design PID controllers for each and see if we can judge dominance of variable from the closed-loop *step* response of all the system (Controller with plant).

In MATLAB/Simulink, the set-point tracking control configuration shown in Fig.5 was design and simulated for all plants (37-40). Simulation results are presented in Fig. 6.

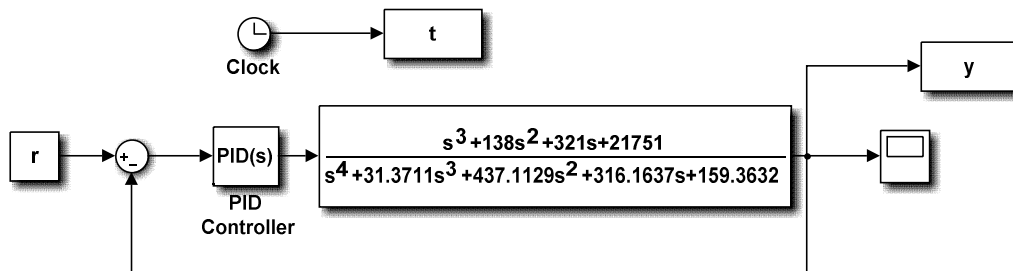


Fig. 5. A typical PID controller design in MATLAB/Simulink

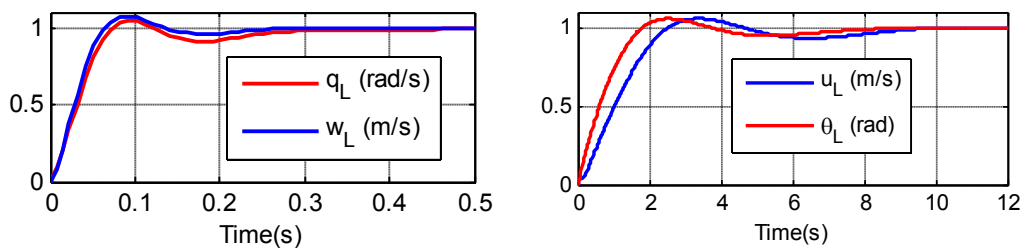


Fig. 6. Closed-loop *step* response of PID controlled longitudinal model variables

3.1 Transient Response

In control system design, an open loop system analysis of the transient response is essential as done in section 2.0. It is also imperative to compute and analyse the transient response of the closed-loop plant in combination the PID control algorithm. In general, analysis of the transient response of such systems to a reference input is difficult. Hence formulating a standard means of assessing transient performance becomes complicated. In many cases, the response is dominated by a pair of poles, thus acts like a second-order system [15]. For a reference step input to a dynamic system, four of the critical parameters that are used to compute transient response could be shown to have the following formulation:

Rise time (t_r), this gives an idea of how fast the system responds to an input,

$$t_r \approx \frac{1+1.1\zeta+1.4\zeta^2}{\omega_n} \quad (41)$$

Settling time (t_s), reveals when the dynamic system reaches a steady values with time.

$$t_s \approx \frac{3}{\zeta\omega_n} \quad (42)$$

Percentage Overshoot (PO), gives the quantity in percentage of how much the system grows beyond or under the reference/tracking signal.

$$PO = \frac{n\pi}{\omega_n \sqrt{1-\zeta^2}}, \quad (43)$$

where, $n= 0,1\dots$, if odd then an overshoot is expected and if n is even an undershoot occurs. For a tracking controller configuration, as used in this study, *Steady-State Error* (SEE), is a measure of the accuracy of the output $y(t)$ in tracking the reference input $r(t)$. Other configurations with different performance measures would result in other definitions of the *steady-state error* between two signals. From Fig. 5, the error $e(t)$ is

$$e(t) = r(t) - y(t), \quad (44)$$

and the steady-state error is

$$e_{ss}(t) = \lim_{x \rightarrow \infty} e(t) = \lim_{x \rightarrow 0} sE(s). \quad (45)$$

Assuming the limit exists, where $E(s)$ is the Laplace transform of $e(t)$, and s is the Laplacian operator, with $G(s)$ the transfer function of the system and $H(s)$ the transfer function of the controller, the transfer function between $y(t)$ and $r(t)$ is found to be

$$T(s) = \frac{G(s)H(s)}{1 + G(s)H(s)}, \quad (46)$$

with

$$E(s) = \frac{R(s)}{1 + G(s)H(s)}. \quad (47)$$

Table 2. Result of PID controllers for longitudinal dynamics

S/N	Plant	Controllers				Transient response			Stability	
		P	I	D	N	t_r (s)	ts (s)	PO(%)	GM	PM
1	$G_{u_L}(s)$	0.015	0.01	0.01	101.8	1.79	8.85	5.78	Inf	60°
2	$G_{\theta_L}(s)$	-0.16	-0.12	0.001	142.7	1.30	7.4	5.71	39	68°
3	$G_{q_L}(s)$	-0.04	-4.21	0	100	0.05	0.25	6.60	Inf	60°
4	$G_{w_L}(s)$	-0.19	-2.53	-0.003	118.7	0.04	0.23	7.22	Inf	60°

With the formulation in (42), we computed the settling time for both the open-loop *phugoid* mode and *short period* mode as;

$$t_{s,sh} \approx \frac{3}{\zeta\omega_n} = 0.19s, \quad (48)$$

$$t_{s_{ph}} \approx \frac{3}{\zeta\omega_n} = 8.06s. \tag{49}$$

Transforming the state-space phugoid and short period mode models, into appropriate transfer functions gives the following:

$$G_{q_{sh}}(s) = \frac{q(s)}{\eta(s)} = \frac{-244.2s^2 - 2220.79521}{s^2 + 30.630s + 413.486}, \tag{50}$$

$$G_{w_{sh}}(s) = \frac{w(s)}{\eta(s)} = \frac{-4.5s - 5334.6}{s^2 + 30.630s + 413.486}, \tag{51}$$

$$G_{\theta_{ph}}(s) = \frac{\theta(s)}{\eta(s)} = \frac{0.0276}{s^2 + 0.74 + 0.3677}, \tag{52}$$

$$G_{u_{ph}}(s) = \frac{u(s)}{\eta(s)} = \frac{0.74}{s^2 + 0.74 + 0.3677}. \tag{53}$$

PID controllers were also designed using the same configuration presented in Fig. 5, and the results are as shown in Fig. 7 and Table 3.

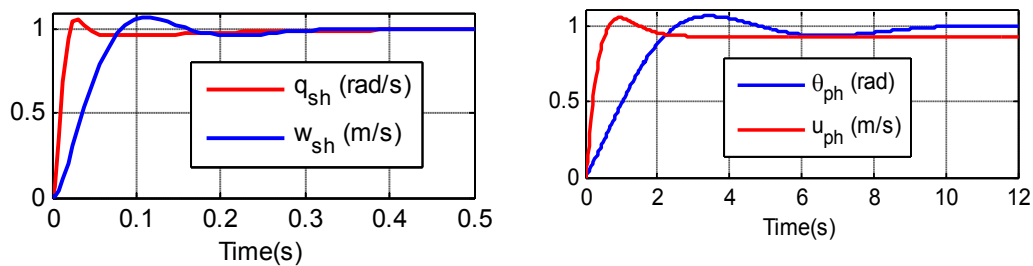


Fig. 7. Closed-loop step response of PID controlled Phugoid and short period mode variables

Table 3. Result of PID controllers for phugoid and short period modes

S/N	Plant	Controllers				Transient response			Stability	
		P	I	D	N	t _r (s)	ts(s)	PO(%)	GM	PM
1	$G_{u_{ph}}(s)$	4.1	7.1	-0.1	36.8	0.38	2.07	12.8	Inf	72°
2	$G_{\theta_{ph}}(s)$	27.5	11.1	15.4	100.6	1.84	8.94	6.6	Inf	60°
3	$G_{q_{sh}}(s)$	-0.38	-11.8	0.002	210.3	0.012	0.19	6.3	Inf	64°
4	$G_{w_{sh}}(s)$	-0.14	-2.1	-0.002	95.9	0.06	0.26	7.0	Inf	60°

We proceed with a graphical comparison of the results of the PID controllers designed for each transfer function in the *short period mode*, *phugoid mode* and longitudinal model. This is depicted in Fig. 8 below.

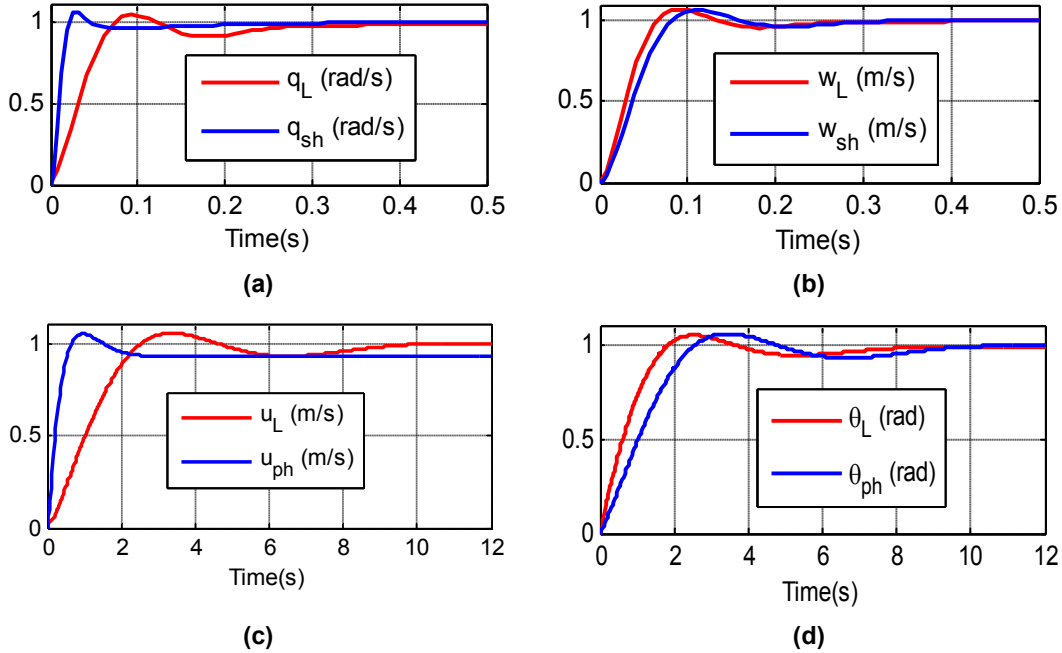


Fig. 8. Comparative plot of closed-loop step response of PID controlled phugoid, short period mode and longitudinal dynamics variables

4. DISCUSSION OF RESULTS

When the full longitudinal model of the UAV in (17) was separated into the phugoid mode and short period mode dynamic equations, their eigenvalues remained the same as seen in (19), (23) and (30) respectively. But their DC gain values vary as presented in (20), (27) and (34) hence; the open-loop responses of the three systems are different (see above Fig. 2, Fig. 3 and Fig. 4).

All designed controllers have appreciably and accepted characteristics as seen in Fig. 8 and from above Table 2 and 3. Attention needs to be drawn to the fact that the plants $G_{uL}(s)$ and $G_{\theta L}(s)$ have the largest settling time, t_s ($t_s = 8.85s$ and $t_s = 7.4s$), its value should be juxtaposed with $t_{sph} = 8.06s$ in (49). Also, the plants $G_{qL}(s)$ and $G_{wL}(s)$, both have a settling time of $t_s = 0.25s$ and $t_s = 0.23s$ respectively, comparing them with the value $t_{ssh} = 0.19s$ as given in (48). Comparing the PID controllers designed for the same state variables in the short period mode and the phugoid mode with those of the longitudinal dynamics of the UAV (Fig. 8), reveals the following; the state variables q_L and q_{sh} have different t_r (with values, 0.05s, 0.012s respectively) and t_s (0.25s, 0.19s respectively),

as shown in Fig. 8a. The state variables w_L and w_{sh} also differ with t_r (with values, 0.04s, 0.06s respectively) and t_s (0.23s, 0.26s respectively) as shown in Fig. 8b. While u_L and u_{ph} have three characteristic terms in disparity, these are, t_r (1.79s, 0.38s respectively), t_s (8.85s, 2.07s respectively) and a steady-state-error of 0.07, this is shown in Fig. 8c. Finally, the pitch angles, θ_L and θ_{ph} vary with t_r (1.3s, 1.84s, respectively) and t_s (7.4s, 8.94s respectively), as shown in Fig. 8d.

5. CONCLUSION

One of several challenges a control system engineer faces is to compensate accurately for disturbances in autopilot design of UAVs. From results in Figs. 2, 3 and 4 above, the *short period* dynamics equation and the *phugoid mode* equations differ from the longitudinal model in terms of DC gain and hence in compensator (controller) requirement as shown in Fig. 8. This simply means that a control algorithm designed to compensate for either *short period* disturbance or *phugoid mode* will be most appropriate if the design is done from the standpoint of their individual mathematical models rather than from the longitudinal model. Also in this study we were able to show that the variables dominating the

system dynamics of a state-space longitudinal dynamics of a UAV can be directly identified after designing PID controllers for each variable, and assessing their step response characteristics. From the *step* response characteristics of the closed-loop system with PID controllers, the *settling time* (t_s) of each system (plant and PID controller) corresponds to the order of the settling times t_{ssh} or t_{sph} measured from the *short period* and *phugoid* mode respectively. Thus the *settling times* (t_s) in the longitudinal plants ($t_s = 8.85s$ and $t_s = 7.4s$) are compared with $t_{sph}=8.06s$, this identifies the output variable of the plants $G_{uL}(s)$ and $G_{\theta L}(s)$ as the *phugoid* variables. Likewise the longitudinal plants with settling times $t_s = 0.25s$ and $t_s = 0.23s$ when compared with $t_{ssh}= 0.19s$, identifies the output variables of the plants $G_{qL}(s)$ and $G_{wL}(s)$, as the *short period* variables.

The common time response characteristic in disparity for all synthesised controllers in this study is the rise time, t_r . In control system design, the smaller the t_r the better the response of the autopilot system. On this basis, we conclude the following; to design a pitch (θ) autopilot the longitudinal dynamic transfer function ($G_{\theta L}(s)$) should be selected as the plant and for pitch rate, q , the short period mode transfer function ($G_{qsh}(s)$) should be selected. For the velocity u autopilot, the phugoid mode transfer function ($G_{uph}(s)$) should be used, and for velocity w autopilot the longitudinal dynamics transfer function ($G_{wL}(s)$) will be the appropriate plant.

ACKNOWLEDGMENTS

The authors will like to appreciate Prof. Li Tao, Fuxin Mingwei Electronics and Technology Co. Ltd.

COMPETING INTERESTS

Authors have declared that no competing interests exist.

REFERENCES

- Dongwon Jung. Hierarchical path planning and control of a small Fixed-Wing UAV: Theory and experimental validation. PhD Dissertation, Georgia Institute of Technology; 2007.
- Houghton EL, Carpenter PW, Steven H. Collicott. Aerodynamics for Engineering Students. Butterworth-Heinemann ISBN: 978-0-08-096632-8; 2013.
- Turkoglu K, Ozdemir U, Nikbay M, et al. PID parameter optimization of an UAV longitudinal flight control system. World Academy of Science, Engineering and Technology. International Journal of Mechanical, Industrial Science and Engineering. 2008;2(9):24-29.
- Kada B, Ghazzawi Y. Robust PID Controller Design for an UAV Flight Control System, in Proceedings of the World Congress on Engineering and Computer Science, WCECS 2011, San Francisco, USA. 2011;2.
- Vaglianti B, Hoag R, Niculescu M. Piccolo system user guide. Cloud Cap Technology. Available:http://www.cloudcaptech.com/resources_autopilots.shtml, 1.3.2 edition, April 2008
- MicroPilot, MP2028 g Installation and Operation; 2005. Available:<http://www.micropilot.com/Manual-MP2028.pdf>
- Bennett S. Nicolas Minorsky and the automatic steering of ships. Control System Magazine, 0272-1708/84/100-0010S01.00© 1984 IEEE; 1984.
- Niler Lwin, Hia Myo Tun. Implementation of flight control system based on Kalman and PID controller for UAV. International Journal of Scientific & Technology Research. 2014;3(4). ISSN 2277-8616. Available:www.ijstr.org
- Cook M. Flight dynamics principles. Elsevier Ltd., 2nd ed.; 2007.
- Murch A. UAV Research Group. Available:<http://www.uav.aem.umn.edu>
- Ridland DM. The longitudinal frequency response to elevator of an aircraft over the short period frequency range. Ministry of Aviation Aeronautical Research Council. C.P. No. 476(21,607) A.R.C. Technical Report, London; 1960.
- Albaker BM, Rahim NA. Flight path PID controller for propeller driven fixed-wing unmanned aerial vehicles; 2011.
- Graham C, et al. Control System Design. Centre for Integrated Dynamics and Control University of Newcastle, NSW 2308 Australia; 2000.

14. Ashish Tewari. Advance control of aircraft, spacecraft and rockets. John Wiley & Sons, Ltd; 2011. ISBN 978-0-470-74563-2.
15. Brogan, et al. Control systems: The electrical engineering handbook. Boca Raton: CRC Press LLC; 2000.

© 2015 Aliyu et al.; This is an Open Access article distributed under the terms of the Creative Commons Attribution License (<http://creativecommons.org/licenses/by/4.0>), which permits unrestricted use, distribution, and reproduction in any medium, provided the original work is properly cited.

Peer-review history:
The peer review history for this paper can be accessed here:
<http://sciencedomain.org/review-history/9899>